

Tests of a large air-core superconducting solenoid as a nuclear-reaction-product spectrometer

R. L. Stern, F. D. Becchetti, T. Casey,^{a)} J. W. Jänecke, P. M. Lister,^{b)} and W. Z. Liu

Department of Physics, University of Michigan, Ann Arbor, Michigan 48109

D. G. Kovar, R. V. F. Janssens, M. F. Vineyard,^{c)} and W. R. Phillips^{d)}

Argonne National Laboratory, Argonne, Illinois 60439

J. J. Kolata

Department of Physics, University of Notre Dame, South Bend, Indiana 46556

(Received 6 February 1987; accepted for publication 23 March 1987)

An air-core superconducting solenoid, with a diameter of 0.2 m and a length of 0.4 m, has been configured for use as a heavy-ion reaction-product spectrometer ($E/A \leq 5$ MeV/u) near $\theta = 0^\circ$. The spectrometer has a large solid angle (10–35 msr) and properties suitable for time-of-flight measurements with flight paths ≥ 2 m. The performance of the spectrometer was established using α -particle sources and nuclear-reaction products from heavy-ion collisions. The characteristics of air-core magnets are compared to those of steel-yoke magnets. The simplicity and ease of operation of the air-core magnet, without significant problems from the (axial) fringe fields, suggests that larger air-core magnets with $d\Omega \geq 20$ msr and capable of focusing ions with $E/A \geq 30$ MeV/u are feasible. Other applications of solenoids and combinations of solenoids with radial electric-field lenses (ELCO lenses) are also discussed, including designs which focus more than one charge state simultaneously.

INTRODUCTION

There are a number of experiments which require large solid-angle devices, often utilizing time-of-flight for mass identification, with the capability of making measurements at or near 0° . Among these are the study of rare nuclear decay modes, such as ^{14}C , ^{18}O , and ^{22}Ne emission,¹ and the study of low cross section, heavy-ion-induced transfer and fragmentation reactions. The transfer reactions can be used to produce neutron-rich nuclei, e.g., via (^{14}C , ^{16}O), (^{18}O , ^{18}Ne), (^{18}O , ^{14}O), etc.,^{2–4} while the fragmentation reactions yield rare, short-lived nuclei.⁵ At $E/A \geq 10$ MeV/u, the transfer and fragmentation reaction cross sections often become forward peaked, with maxima typically at angles less than 20° . In addition, when a heavy-ion beam is incident on a lighter target, inverse kinematics concentrates the reaction products at forward angles.

A device which can satisfy many needs for a $\theta \approx 0^\circ$ reaction product collector is the superconducting solenoid spectrometer.^{6,7} The solenoid, when aligned at $\theta \approx 0^\circ$, acts as a large-aperture, broad-range lens ($d\Omega > 10$ msr) with nearly isochronous flight paths. Solenoids have been shown to be useful for studies of transfer reactions^{6,7} and rare nuclear decays.⁸ They also should have applications in measurements of particle-particle and particle-gamma correlations,⁶ the production of secondary, radioactive beams,⁹ and the detection of energetic charged mesons (π^\pm , K^\pm) and electrons (β^\pm). The latter could be detected simultaneously in a solenoid configured as a pair spectrometer. Also, long solenoids, individually or together with radial electric field (ELCO) lenses,^{10,11} appear to have some interesting properties that would make them useful as wideband nuclear-reac-

tion-product collectors. Thus there are numerous applications for this type of device.

I. SOLENOID SPECTROMETERS

A. Advantages of solenoid optics

Solenoid spectrometers have, in addition to their solid angles, certain advantageous optical features compared to dipole-magnet spectrometers. These include variable object/image distances and, hence, variable magnification, dispersion, and flight path. Also, the image can be focused to a small disk, limited only by high-order aberrations.¹² This simplifies the design of the focal-plane detection system. As an example, one can use silicon surface-barrier detectors for position, ΔE , E , and time-of-flight (TOF) measurements (see Sec. II E). However, since a solenoid has low momentum dispersion and non-negligible spherical aberrations at the focal plane, it is difficult to determine accurate ion energies (momenta) from radial or axial position measurements alone.

Large superconducting-solenoid magnets are relatively easy to construct and are available commercially at modest cost. When used without a steel yoke, as in our device, they are lightweight and, hence, easily transported and moved. As an example, our magnet can be installed and aligned for an experiment, or removed, in less than a day.

B. Air-core versus steel-yoke designs

The Orsay group^{6,8} has described the construction and operation of a 0.2-m bore, 3-T solenoid spectrometer which utilizes a large steel yoke to minimize the fringe fields and to

TABLE I. Comparison of air-core relative to steel-yoke solenoid spectrometers.

Advantages:	
(1)	Relatively low cost
(2)	Easy to design and construct large-bore magnets
(3)	Available commercially
(4)	Simple cryostat design with long hold time
(5)	Field is easily calculable and scales linearly with current
(6)	No hysteresis or saturation
(7)	Extremely stable field when run in persistent mode
(8)	Low weight, hence transportable
(9)	Low weight, hence easily rotated with respect to beam axis
(10)	Easily reconfigured with different focal lengths, dispersion, and solid angles
Disadvantages:	
(1)	Fringe fields present near target and detector
(2)	Nonmagnetic components and environment are required
(3)	Slightly less focusing power for a given coil design
(4)	Exposed cryostat and magnet (safety)

clamp the entrance and exit fields. However, if one can tolerate fringe fields of a few hundred gauss at a distance of ~ 1 m from the magnet, i.e., at typical target and detector locations, there appear to be no significant advantages to the yoked magnet relative to the simple air-core design. A comparison of the two designs is given in Table I. It should be noted that when the solenoid is configured at $\theta \doteq 0^\circ$, its fringe fields at the target and detector are mostly axial ($B = B_z$) and thus do not deflect the beam, which is traveling in the axial direction. In practice there is some misalignment of the optical, magnetic, and beam axes, so some minor beam steering is necessary to keep the beam accurately centered (± 1 mm) at high magnetic fields. Most detectors (e.g., solid-state detectors, scintillators, and high-field proportional counters) are not greatly affected by the axial fringe fields, and those that are affected (e.g., photomulti-

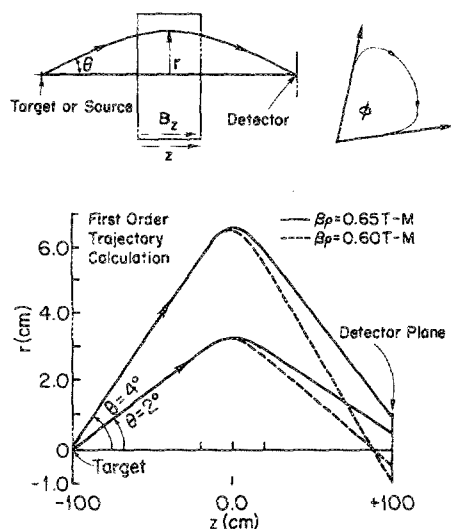


FIG. 1. Top: Geometry of the solenoid spectrometer and corresponding particle trajectories. The angle ϕ is the spiral angle of the ion orbit from target (object) to detector (image). Bottom: A set of calculated ion trajectories [Eq. (2)] for a range of energies and scattering angles (see, also, Table IV). Note the different vertical and horizontal scales.

TABLE II. Properties of the solenoid magnet.

Magnet coil length ^a	34 cm
Magnet coil ^a i.d.	24 cm
o.d.	27 cm
Effective thin sheet coil ^b diam	24 cm
length	35 cm
Inductance	~ 12.5 H
Stored energy (at 3.5 T)	~ 100 kJ
Central field (at 4.2 K)	3.5 T @ 125 A
Power supply	IGC-180 M (± 4 V, 180 A)
Ramp time (0–3.5 T)	25 min
Decay rate (persistent mode)	$< 10^{-4}$ /h
Cryostat length ^a	46 cm
Cryostat bore (warm) ^a	20 cm
Cryostat capacity ^a	10 l
LHe to cool down	50–70 l
LHe to refill	15 l
Power leads	LHe vapor cooled, nonretractable
Cryostat shielding	LHe vapor inner shield, LN outer shield
Hold time (nonpersistent mode)	20 h

^aIntermagetics General Corp. model 31010.

^bDimensions of current sheet needed to reproduce the measured axial magnetic field (Fig. 2).

plier tubes and ion chambers) can usually be locally shielded without disturbing the ion images at the focal plane. This might be more of a problem with very large-bore, high-field solenoids, but has yet to be a significant problem with smaller magnets.

The minor disadvantages of the air-core design are greatly offset by the numerous advantages (see Table I); the device is simple to construct, can have an efficient cryostat, is easy to move in and out of an accelerator beam line, and is easy to reconfigure for a particular experiment. Furthermore, the magnetic field and, hence, the optical properties scale exactly with the current with no hysteresis. This greatly simplifies the calibration and operation over a large variation of magnetic field. In our magnet, the field can be varied from 0 to 3.5 T in about 30 min, with typical field changes ($\pm 20\%$) taking only a few minutes. We thus consider the air-core solenoid design to be advantageous and very cost effective relative to the steel-yoke magnet design, particularly for large-bore magnets.

C. Ion optics of solenoids

The optics of a solenoidal ion lens are described in the literature.^{12,13} Solenoids have been used for many years as large solid-angle electron spectrometers^{14,15} and more recently as heavy-ion spectrometers,^{6,7} following earlier suggestions^{16,17} for this application.

Briefly, ions emitted at an angle θ from a target, located as shown in Fig. 1, spiral through the magnet (spiral angle $\equiv \phi$) and in first order are brought back to a focus at the image plane. A short solenoid has an equivalent thin-lens focal length given^{12,13} by

$$1/f = \overline{B_z^2} L / 4(B\rho)^2, \quad (1)$$

where $\overline{B_z^2}$ is the mean-square axial field, L is the corresponding effective solenoid length, and $B\rho$ is the ion's mag-

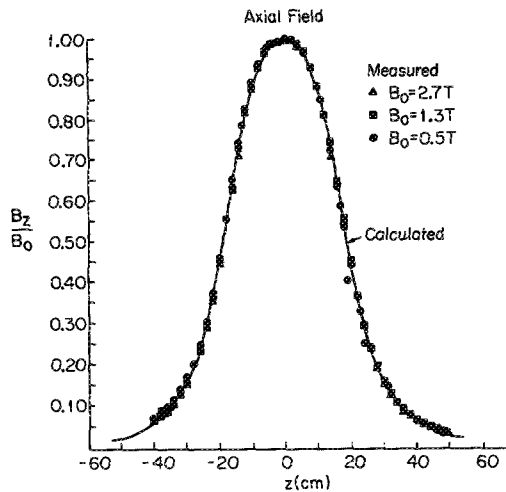


FIG. 2. A comparison of the measured and calculated axial field $B_0(z)$. The calculations use a thin current sheet approximation (see Table II).

netic rigidity. The latter is proportional (nonrelativistically) to the ion's momentum p divided by its charge state q , that is, p/q or \sqrt{ME}/q , where E is the ion's kinetic energy. Again, in first order, the ion's radial r and azimuthal ϕ motions are given by

$$\frac{d^2r}{dz^2} + \left(\frac{B_z}{2(B\rho)} \right)^2 r = 0, \quad (2)$$

$$\frac{d\phi}{dz} = - \frac{B_z}{2(B\rho)}, \quad (3)$$

where $B_z = B_0(z)$ is the central magnetic field as a function of z , the axial position (see Fig. 1). One can show^{12,13} that the spherical aberrations vary as θ^3 and produce not a point

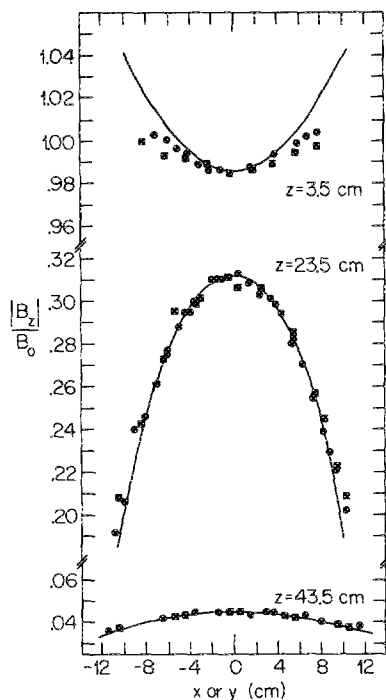


FIG. 3. Measured and calculated off-axis magnetic fields.

TABLE III. Univ. of Michigan 20-cm bore spectrometer characteristics.

Target to solenoid center	99 cm
Detector to solenoid center	96 cm
Aperture to solenoid center	81.5 cm
Angular range	1° - 6°
Maximum solid angle (1° - 6°)	33 msr
Typical solid angle ($\theta = 3^\circ$ - 6°)	25 msr
Maximum particle energy ($\theta = 4^\circ$, 3.5 T)	$20 q^2/A$ MeV
Radial dispersion at detector ($\theta = 4^\circ$)	4% $(\Delta p/p)/\text{cm}$
Axial (z) dispersion at detector ($\theta = 4^\circ$)	0.3% $(\Delta p/p)/\text{cm}$
Energy range for 4-cm-diam detector ($\theta = 4^\circ$)	20%-30%
Effective focal length (thin lens approximation)	42 cm
	(@ $B\rho = 0.62$ T m)
Flight path ($\theta = 4^\circ$)	1.95 m
Nonisochronism ($\theta = 3^\circ$ - 6°)	0.5%
Spiral angle, ϕ (at $B\rho_{\text{max}}$)	68°
Circle of least confusion (3° - 6°)	1.3-cm diam

image, but instead an image contained in a small circle of least confusion, which then determines the minimum detector size.

With an air-core magnet of known coil dimensions and current density, $B_0(z)$ can be calculated analytically to high accuracy and the off-axis field $B(r, \phi, z)$ found using appropriate expansions.^{12,13} In practice it is usually sufficiently accurate to approximate the actual coil by a thin current sheet with dimensions chosen to reproduce $B_0(z)$. Ion orbits can be easily calculated by numerical integration of (2) and (3) or by ray tracing,^{12,18} which then permits the determination of transmission curves (see Sec. III A), image size and location, image aberrations, and the axial and radial dispersions.

II. THE UNIVERSITY OF MICHIGAN 20-CM BORE SUPERCONDUCTING-SOLENOID SPECTROMETER

A. Magnet

We have assembled a 20-cm bore solenoid spectrometer utilizing one of several superconducting Faraday-rotator magnets obtained as surplus from the U. S. Department of Energy laser-fusion program. These are commercially built¹⁹ air-core magnets, with characteristics as shown in Table II. In accelerator experiments the magnet is normally run in the nonpersistent mode. This increases the LHe boil off by 10%-20% relative to persistent mode operation.

B. Field profile

The axial and off-axis magnetic fields, $B_0(z)$ and $B(x, y, z)$, were mapped with Hall probes located at the end of a long aluminum shaft fastened to an x - y - z drive. Initial measurements²⁰ were done with a single-axis probe. Later measurements were done with a specially constructed three-axis probe (B_x, B_y, B_z) made up of three small (9.5×31.8 mm²) Hall-probe chips²¹ mounted at right angles to each other. Voltages were read out through a common signal conditioner via a CAMAC ADC computer system. A set of measured fields is shown in Figs. 2 and 3. Figure 2 shows the measured axial field and the values calculated using the thin-sheet approximation (see Table II). Up to distances of ± 1 m from the magnet, these agree to about 3%, which is suffi-

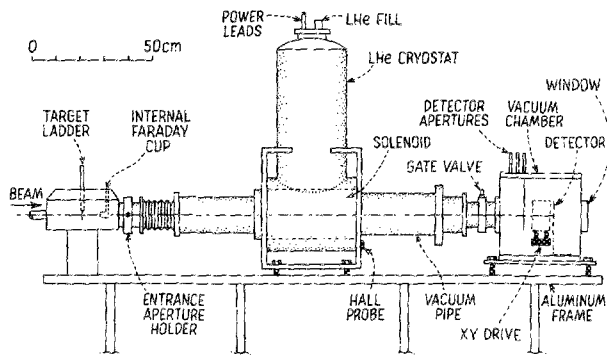


FIG. 4. The layout of the Univ. of Michigan 20-cm bore solenoid spectrometer.

cient for most purposes [Eq. (1)].

Measurements of B_x and B_y (see Fig. 3) indicate that the optical (i.e., cryostat bore) and magnetic axes differ slightly, with the latter at an angle of about 1° to the former. This is not surprising since these magnets were used as Faraday rotators and, therefore, were not specified to have a highly concentric cryostat bore and coil. This slight misalignment then leads to an ion image centered about 1 cm off the optical axis.

The fringe fields near the magnet exhibit the typical $1/r^3$ falloff expected for an equivalent magnetic dipole. The fringe fields are generally not a major problem except close ($< \frac{1}{2}$ m) to the magnet. As operated, the magnet is ≈ 1.5 m from any steel structures, e.g., structural steel support beams, floor mesh, vacuum pumps, beam-line supports, beam steerers, and quadrupole magnets. Items affected by the fringe fields

(TV cameras, ion gauges, etc.) are locally shielded with μ metal and are far enough away to have little or no effect on the ion optics or magnet operation.

C. Spectrometer configuration

The magnet was configured for use as an ion spectrometer, as shown in Fig. 4, with the characteristics given in Tables III and IV. The scattering chamber, solenoid, and detector vacuum chamber were mounted via adjustable non-magnetic bolts on a simple aluminum frame made up of ca. 6×6 cm aluminum angle and ~ 2 -cm-thick aluminum mounting plates. The scattering angles (see Fig. 1) were defined by an appropriate aperture located on a sliding panel of apertures 18 cm from the target. The beam was stopped in a small, movable, carbon or brass Faraday cup designed to minimize scattering into the solenoid, which can be a problem at small angles if the beam moves off center. A set of special apertures was used to study some of the optical properties of the spectrometer.^{7,18}

The detector (see Sec. II E) was mounted on a small xy platform driven manually via flexible shafts exiting the chamber through CAJON fittings,²² with potentiometer position readouts. Likewise, a set of detector apertures and calibration-source holders (see Fig. 4) were manually operated via CAJON feedthroughs. Recent experiments have employed a rotating detector collimator system, which also includes a small solid-state detector for use in tuneup, ion identification, and minimization of background sources.

The magnetic field is primarily monitored and regulated to one part in 10^3 by the magnet current supply, with a Hall

TABLE IV. Energies and TOF ranges for Univ. of Michigan solenoid spectrometer ($B_0 = 3.5$ T).

Particle	A	q^a	Maximum E_{lab} Range ^b (MeV)	\bar{E}/A (MeV/u)	Radial Dispersion ^c (% E/cm)	TOF range ^d (ns)
Sn	118	50+	376-473	3.6	9.3	50.9-45.3
		25 ^e	94.1-118.5	0.9	9.3	156.2-139.2
Ni	58	21 ^{+e}	135.0-170.0	2.6	9.3	91.4-81.5
		21 ⁺	130.5-164.3	2.5	9.3	94.6-84.3
Ca	40	8 ^{+e}	143.8-180.8	4.0	9.3	73.6-65.6
		20 ⁺	177.4-223.1	5.0	9.3	66.2-59.1
S	32	16 ⁺	141.9-178.5	5.0	9.3	66.2-59.1
Ne	18	10 ^{+e}	98.5-123.9	6.2	9.3	59.6-53.2
		10 ⁺	88.7-111.6	5.0	9.0	66.2-59.1
O	14	8 ^{+e}	81.0-101.9	6.5	9.3	58.0-51.7
		8 ⁺	71.0-89.3	5.0	9.0	66.2-59.1
C	12	6 ^{+e}	54.9-64.5	5.0	9.0	65.2-60.2
		3 ^{+e}	22.8-28.7	3.7	9.4	77.3-68.9
Li	7	3 ⁺	20.0-25.1	2.8	9.2	83.2-78.7
		3 ⁺	20.0-25.1	2.8	9.2	83.2-78.7
He	4	2 ⁺	17.7-22.3	5.0	9.4	66.2-59.0
H	3	1 ⁺	5.9-7.5	2.2	9.8	99.5-88.2
H	1	1 ⁺	17.6-22.1	19.9	9.3	33.2-29.7
K ^{+e}	—	1 [±]	32.5-40.6	—	9.0	17.8-15.9
π^{+f}	—	1 [±]	89.8-107.8	—	7.3	8.1-7.8
e^\pm	—	1 [±]	181.5-203.7	—	4.4	6.4-6.4

^a Ion charge state.

^b Ion energy range covered by a 2.76-cm-diam (600 mm²) focal-plane detector, e.g., a large Si solid-state detector (see Sec. II E).

^c The ion energy dispersion in the xy focal plane (see Fig. 1).

^d The ion TOF range corresponding to the ion energy range indicated with $\theta = 4^\circ$. The TOF dispersion (nonisochronism) is typically 0.15%/deg (see Table III).

^e Equilibrium charge state, in a target foil, for ions of energies indicated.

probe (see Fig. 4) used for secondary measurements. The spectrometer focal plane is determined by using a ^{228}Th α source ($E_\alpha = 5.34\text{--}8.78$ MeV) located on the target ladder. The magnet current is then appropriately scaled with $B\rho$ to focus other ions.

Vacuum is provided by a portable turbo pump or cryo-pump mounted on the scattering chamber ≈ 1 m from the magnet. These pumps and most of the valves and beam-line components are constructed of mostly nonmagnetic materials, viz. aluminum or nonmagnetic stainless steel, and hence can be used near the magnet. The vacuum in the present system is $\sim 2 \times 10^{-6}$ Torr and appears to be partially limited by the solenoid entrance apertures. A better vacuum (10^{-7} Torr range) would likely require a pump located at the detector box (see Fig. 4), but we have not yet found this necessary.

In some applications, where a high ion collection efficiency is desired and poor energy resolution is tolerable, it may be advantageous to run the spectrometer in a gas-filled mode.²³ This results in the effective collection of more than one charge state. It appears that with suitable baffles and perhaps differential pumping the air-core solenoid spectrometer configuration would be well suited for this mode. However, we have developed alternate schemes for focusing several charge states (see Sec. V).

D. Detection of ions

The detectable range of particle energies and flight times, and the corresponding energy dispersion at the spectrometer focal plane, are given in Table IV. These characteristics are for the configuration shown in Fig. 4 and described in Table III. As noted, the spectrometer is capable of focusing, simultaneously if desired, β^+/β^- , π^+/π^- , and low energy K^+/K^- . The sign of the particle can be deduced by measuring the sign of the spiral angle ϕ (see Fig. 1) either at the focal plane or with xy detectors (e.g., wire chambers)

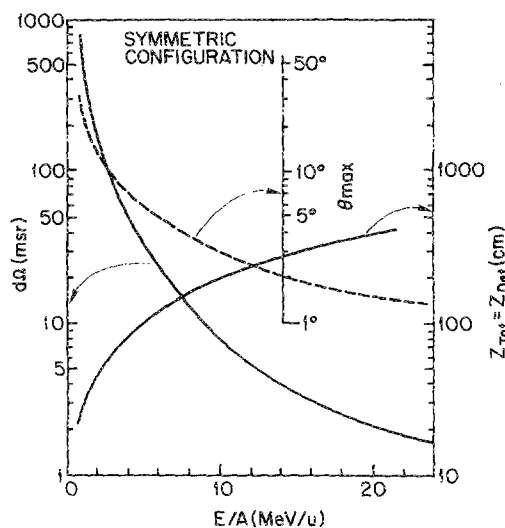


FIG. 5. Calculations of solid angle vs image and object distance and $B\rho$ for the 20-cm bore magnet ($B_0 = 3.5$ T), assuming a symmetric layout. The corresponding energies for nonrelativistic heavy ions with $q = Z = A/2$ are indicated together with the range of accepted scattering angles.

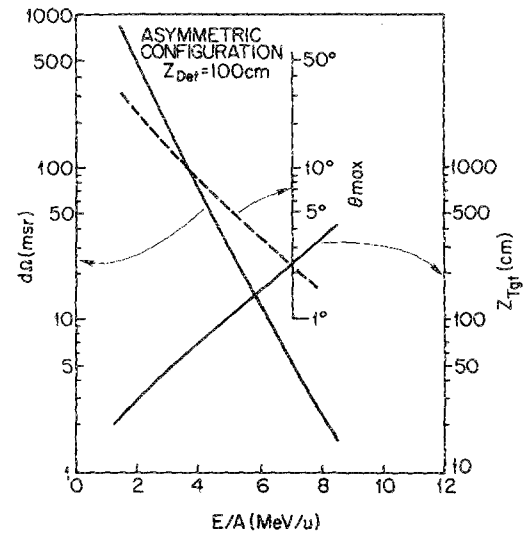


FIG. 6. Same as Fig. 5, but for an asymmetric layout.

located at the entrance and exit of the solenoid, provided they can operate in the magnet's fringe fields. This type of arrangement would also permit the use of the solenoid as a pair spectrometer in reactions where a β^+/β^- or π^+/π^- pair is emitted in a forward cone within the spectrometer's acceptance angle. The short solenoid flight path, which can be made $\lesssim 1$ m, is particularly well suited for π^+/π^- and K^+/K^- detection, since these particles decay in flight with $t_{1/2} \sim 10^{-8}$ s, corresponding to $l_{1/2} \lesssim 3$ m.

As with an optical lens, the dispersion and magnification of a solenoid spectrometer can be changed by varying the detector and object distances, causing a corresponding change in the energy range that can be focused without hitting the magnet cryostat bore (see Fig. 4). Thus the maximum solid angle (or lens $f/\#$) is determined by the geometrical arrangement and the bending limit ($B\rho_{max}$) of the magnet. The relationships for our magnet are shown in Fig. 5 for a symmetric configuration (image distance = object distance; unity magnification) and in Fig. 6 for an asymmetric configuration. The asymmetric mode permits a larger solid

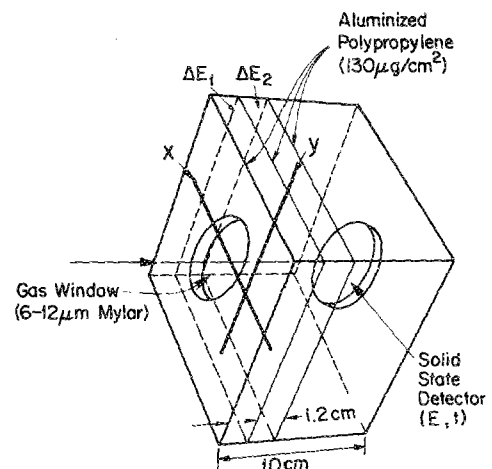


FIG. 7. Schematic diagram of the gas proportional counter silicon solid-state detector system. The former provides xy and ΔE and the latter, E and t .

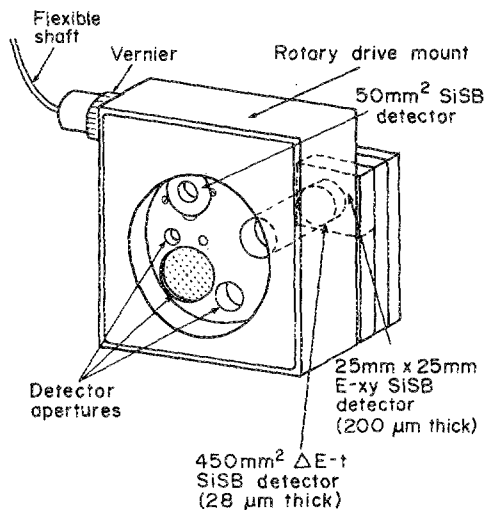


FIG. 8. Diagram of the silicon solid-state $xy - \Delta E - E - t$ detector telescope system.

angle, but at the expense of an increase in magnification for a given E/A (see Sec. IV A).

E. Two-dimensional, heavy-ion, focal plane detectors

In order to uniquely identify a heavy ion at the focal plane, one must deduce its atomic number Z , mass M , energy E , and charge state q . This can be done by determining the ion's $B\rho$ ($\propto \sqrt{ME}/q$), TOF ($\propto \sqrt{M/E}$), $\Delta E/\Delta x$ ($\propto Z^2 M/E$), and E . Determination of $B\rho$ in a solenoid requires a two-dimensional position (xy) readout since point objects image as disks (in focus) or rings (off focus). We have developed two systems to do this: a resistive-wire xy gas proportional counter with a large solid-state detector inside and a two-dimensional position-sensitive solid-state counter telescope.

1. Gas proportional counter

The two-dimensional gas proportional counter is shown in Fig. 7. It consists of two short, 38- μm diam, high-resistance, carbon-covered quartz fibers strung at right angles to each other in a double proportional counter. The electrodes are stretched and aluminized polypropylene foils of about 130 $\mu\text{g}/\text{cm}^2$ thickness. The proportional counter gives x and y (via charge division) and two ΔE signals (via summing left/right and up/down wire signals). The counter is normally operated at 75 Torr of isobutane with +500 to +700 V on the wires. The double ΔE measurement proved useful in minimizing, via double ΔE gating, the Landau ΔE tail arising from intense groups such as inelastically scattered incident beam. The latter can be a severe problem in large solid-angle devices, such as ours, run near $\theta = 0^\circ$. Beam scattering also requires detectors with a high count-rate capability (> 5 K ions/s).

The ion's residual energy and arrival time are determined with a large area (600 or 450 mm^2) silicon detector $\sim 300 \mu\text{m}$ thick. The detector is usually overbiased to im-

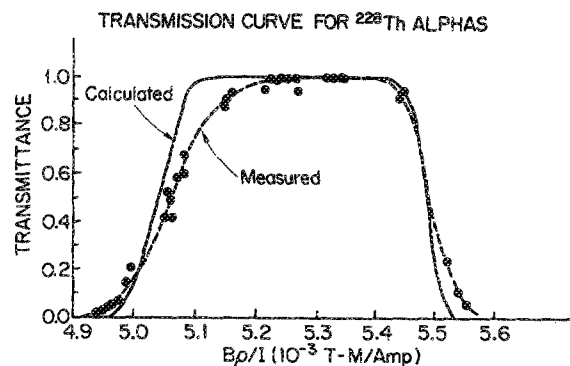


FIG. 9. Measured and calculated solenoid-spectrometer transmission curve for α particles emitted from a ^{228}Th source ($E_\alpha = 5.34\text{--}8.78$ MeV) located at the target position with angular acceptance of $5^\circ\text{--}6^\circ$.

prove charge collection and timing, but the large area limits the TOF resolution to 0.6–1 ns FWHM. This is due to the corresponding large detector capacitance and, hence, slow rise time of ~ 20 ns.

The position resolution for the xy detector (which is operating in a 100- to 200-G fringe field) was typically $\lesssim 2$ -mm FWHM and was limited by the ΔE signal and wire gain. This position resolution is comparable to the spherical aber-

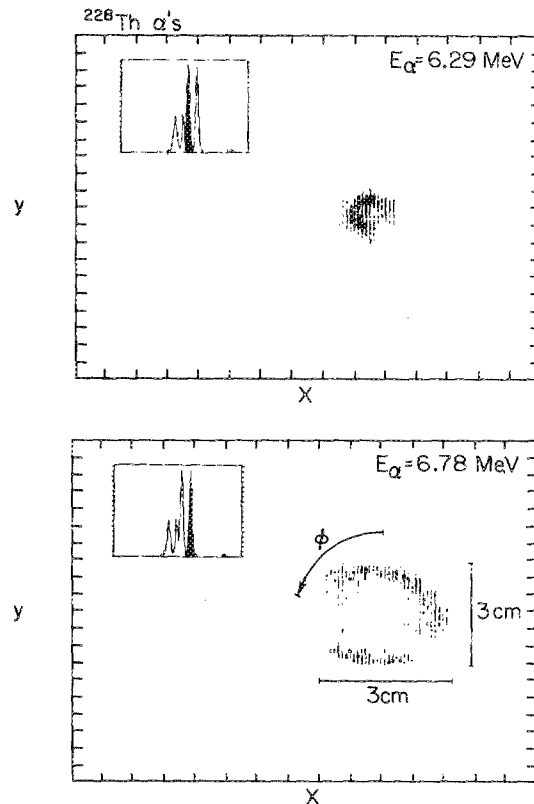


FIG. 10. α -particle images obtained at the solenoid-spectrometer focal plane for specific ^{228}Th groups. These were obtained using the $xy - \Delta E - E - t$ gas proportional counter detector (see Fig. 7) with an energy gate set on the selected α groups as indicated. The on-focus image ($E_\alpha = 6.29$ MeV) represents the circle of least confusion. The off-focus image ($E_\alpha = 6.78$ MeV) is a ring with two small areas blocked off, corresponding to the aperture and Faraday cup supports. Rotation of the image by the spiral angle ϕ is evident. The aperture used was a ring with an opening of $5.2^\circ\text{--}6^\circ$.

rations present and therefore we do not use, as one does with most dipole spectrometers, the $B\rho$ value inferred from xy measurements to determine E accurately. Instead, we use a separate E detector.

While the gas proportional counter system proved adequate for initial imaging⁷ and preliminary studies of transfer reactions,²⁴ it was not optimal for precision energy and Q -value (mass) measurements. This was due to energy straggling in the entrance window, dead gas layer, and foil electrodes. (A design using a thinner entrance window supported by a wire grid, and inner electrodes of high transmission mesh²⁵ might be better suited for energy measurements.) Nonetheless, much of the data presented here were obtained with this relatively simple detector.

2. Two-dimensional solid-state detector telescope

More recent measurements have utilized a ($\Delta E - t$), ($E - xy$) solid-state telescope consisting of a large area (450 mm²), planar, 28- μ m-thick silicon²⁶ detector for ΔE and timing backed by a special 25 \times 25 mm² two-dimensional position-sensitive silicon surface-barrier E detector 200 μ m thick (see Fig. 8). This position-sensitive detector was developed at Lawrence Berkeley Laboratory²⁷ and utilizes a resistive anode for xy position readout. It has a position resolution of <0.7 mm and 90- to 140-keV energy resolution for 8.78-MeV alpha particles. This counter telescope was developed for Q -value and related measurements utilizing the (¹⁸O, ²⁰Ne), (¹⁸O, ¹⁸Ne), and (¹⁸O, ¹⁴O) reactions.¹⁸

III. SPECTROMETER TESTS

A. Transmission curves and α -source images

Initial tests^{7,18,20} involved both axial z and radial xy imaging of ²⁴¹Am ($E_\alpha = 5.49$ MeV) and ²²⁸Th ($E_\alpha = 5.34 - 8.78$ MeV) alpha sources located at the target (object) position (see Fig. 4). Axial imaging was obtained either by moving a small (50 mm²) solid-state detector along the z axis or ramping the magnet field (i.e., current) with the detector located at a fixed z position. With appropriate gating on a particular α -particle energy, one obtains a transmission curve vs $B\rho$ for the spectrometer. Such a curve is shown in Fig. 9. The measured values agree reasonably well with those calculated via ray tracing assuming a uniform point source, although the actual source was a few millimeters in diameter. These data verify the basic operation of the air-core design.

At a fixed field, one can obtain images of the on- and off-

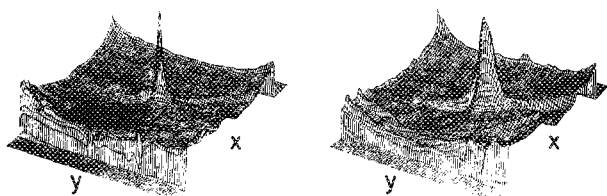


FIG. 11. Focused (left) and unfocused (right) solenoid focal-plane images of 76-MeV ¹⁶O ions scattered from gold, $\theta = 5.2-6^\circ$ (8.6 msr), recorded with plastic track detectors and digitized with a CCD camera.

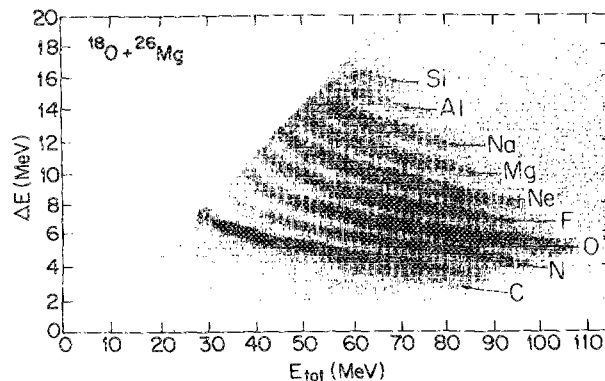


FIG. 12. A $\Delta E - E$ spectrum for 106-MeV ¹⁸O + ²⁶Mg, obtained with the gas proportional counter detector.

focus ion groups by gating on a given ion's energy (i.e., $B\rho$) and observing x and y . A set of images for two specific ²²⁸Th α -particle groups is displayed in Fig. 10. The on-focus group exhibits the disk image ~ 1 cm in diameter expected from the spherical aberrations of the solenoid.^{12,13,18} The off-focus group images as a ring with radius r and width Δr . One can also observe, in the off-focus image, the areas blocked by the Faraday cup and entrance aperture supports, rotated by the spiral angle ϕ (see Fig. 1). As noted previously, we do not use the xy measurements to determine (via $B\rho$) the ion energies, so the image measurement is used primarily for ion identification (M, Z, q) and reducing interference from background. Owing to spherical aberrations, the width Δr of the ring observed for an unfocused monoenergetic ion group is related to the spectrometer's angular acceptance.^{12,13} This can be used to make angle-dependent corrections to the TOF, energy, and other quantities. Thus one can in principle improve the TOF resolution, and thus the mass determination, or the energy resolution (see Sec. III B 3).

B. In-beam tests

1. Images

In-beam tests were performed at the Argonne National Laboratory (ANL) ATLAS booster facility.²⁸ This accelerator provides a pulsed heavy-ion beam, $A \leq 70$, $E \leq 250$ MeV, $\Delta t \leq 300$ ps, with a start-time marker provided by the

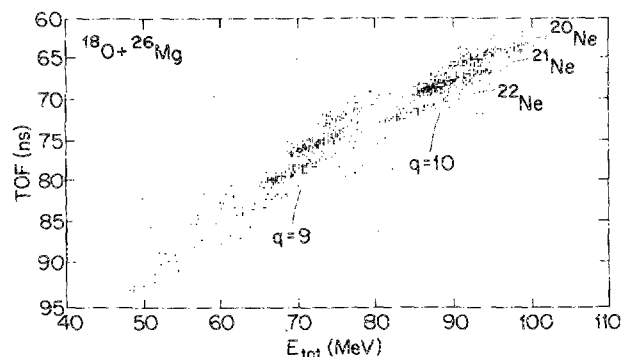


FIG. 13. An E -TOF spectrum for Ne particles for 106-MeV ¹⁸O + ²⁶Mg, $\theta = 3-6^\circ$, obtained with the gas proportional counter detector. An xy gate about the center of the image was applied to separate charge states.

LINAC rf signal. Tests were done on the general purpose beam line using 76- to 106-MeV $^{16,18}\text{O}$ and ^{32}S ions with the detectors described previously (Secs. II E 1 and II E 2) and, in addition, plastic (CRONAR) track detectors.^{29,30} The latter were mounted on a special holder located at the spectrometer focal plane and were used to image on- and off-focus elastic scattering. Images were analyzed off line by scanning the ion-track density in the developed plastic with a CCD camera and digitizing system. This yielded highly focused images (see Fig. 11) only a few millimeters in diameter due in part to the forward-angle weighting of Rutherford scattering ($\propto \sin^{-4} \theta$). Other off-focus images for a variety of different apertures may be found in Refs. 7 and 18. These confirm the optical properties expected for an air-core solenoid as a particle lens.

2. Particle energy spectra

Reaction products were detected and identified using the reactions $^{16}\text{O} + ^{12}\text{C}$, Au at $E = 76$ and 72 MeV; $^{32}\text{S} + ^{27}\text{Al}$, Au at $E = 90$ MeV; and $^{18}\text{O} + ^{26}\text{Mg}$, Ni ^{18}O , ^{110}Pd at $E = 100$ and 106 MeV. $\Delta E - E$ and $E - E$ spectra, with the latter gated via xy to limit the $B\rho$ range, are displayed in Figs. 12 and 13. These were obtained with the gas proportional counter detector (see Fig. 7), which exhibits slight distortions in ΔE vs E due to an apparent dependence of the proportional counter charge-collector efficiency on x and y , i.e., on distance from the anode wires. More troublesome is the Landau spread in ΔE which causes the intense inelastic groups to spill over into adjacent regions. However, this was greatly reduced by employing the double ΔE gating available (see Sec. II E 1), permitting identification and separation of groups up to complete fusion ($Z = 20$).

The mass resolution of the spectrometer is limited by the nonisochronism (see Table IV) vs θ , the kinematic shift vs θ , and the timing resolution of the accelerator and the detector. With $\Delta t = 0.6$ – 1 ns, typical of the gas proportional counter system (see Fig. 13), one has $\Delta M/M \approx 1/50$ for a 2-m flight path.

Higher Z -, M -, and E -resolution spectra were subsequently obtained with the $\Delta E - t - xy - E$ solid-state detector system, again using the ANL ATLAS booster facility

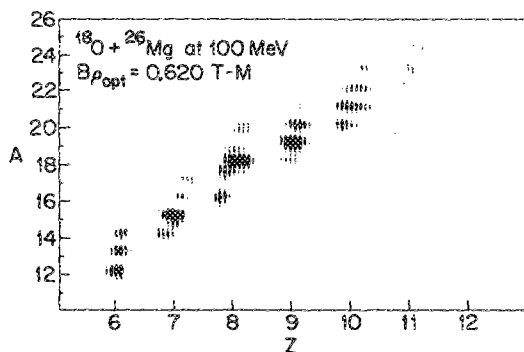


FIG. 14. A Z vs A identification spectrum for 100-MeV $^{18}\text{O} + ^{26}\text{Mg}$, obtained with the position-sensitive SISB $\Delta E - t - xy - E$ detector system. The Z parameter was obtained by linearizing curves in ΔE vs E and the A parameter was obtained by linearizing curves in TOF vs E which were gated on a particular Z group.

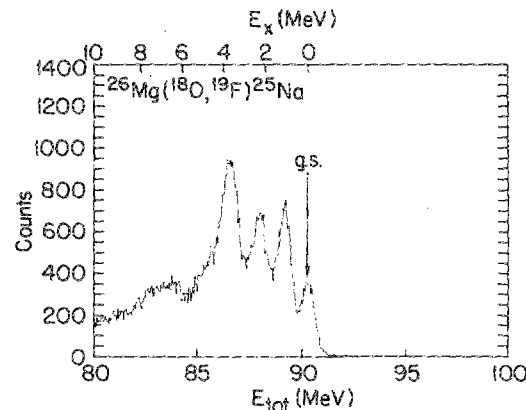
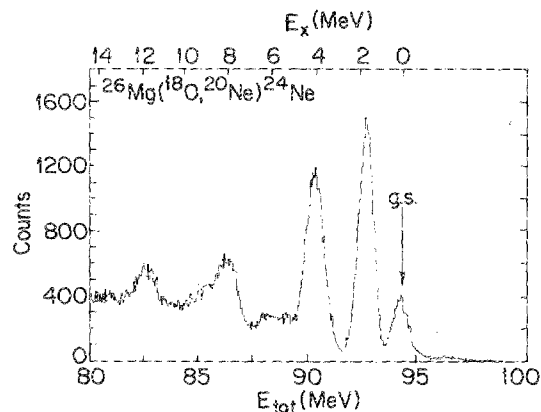


FIG. 15. Top: Energy spectrum for $^{26}\text{Mg}(^{18}\text{O}, ^{20}\text{Ne}) ^{24}\text{Ne}$ at 100 MeV. The angular acceptance was $\theta = 3^\circ$ – 6° ($d\Omega = 25$ msr). Bottom: Energy spectrum for $^{26}\text{Mg}(^{18}\text{O}, ^{19}\text{F}) ^{25}\text{Na}$ at 100 MeV. The angular acceptance was $\theta = 5^\circ$ – 6° ($d\Omega = 8.5$ msr).

with an rf TOF start signal ($\Delta t < 300$ -ps FWHM). These runs were done with a high-magnetic-rigidity incident beam (100-MeV ^{18}O) to avoid the problem of high count rates and background due to the elastically scattered beam. This is the case, for example, when one studies transfer reactions such as $(^{18}\text{O}, ^{20}\text{Ne})$, $(^{18}\text{O}, ^{18}\text{Ne})$, and $(^{18}\text{O}, ^{14}\text{O})$. Unlike the gas detector, there is only a single ΔE measurement, so the Landau ΔE tail can be a problem. At higher ion energies a second

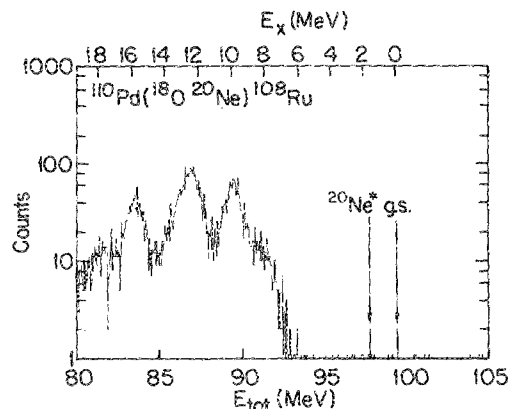


FIG. 16. Energy spectrum for $^{110}\text{Pd}(^{18}\text{O}, ^{20}\text{Ne}) ^{108}\text{Ru}$ at 100 MeV. The angular acceptance was $\theta = 5^\circ$ – 6° ($d\Omega = 8.5$ msr). The $^{20}\text{Ne}^*$ state is at 1.63 MeV.

ΔE detector would be advantageous to minimize this problem. Suitable pulse-shape analysis in either the ΔE or E detectors might also help provide a redundant Z identification—at least for low Z (≤ 10).

A Z vs A identification spectrum for $^{26}\text{Mg} + ^{18}\text{O}$, obtained with the solid-state detector telescope, is shown in Fig. 14. Z and M were determined by linearizing curves in the ΔE vs E and TOF vs E spectra, respectively.

Energy spectra for $^{26}\text{Mg}(^{18}\text{O}, ^{20}\text{Ne})^{24}\text{Ne}$ and $^{26}\text{Mg}(^{18}\text{O}, ^{19}\text{F})^{25}\text{Na}$ are shown in Fig. 15. The former was obtained with a solid angle of 25 msr ($\theta = 3^\circ\text{--}6^\circ$), and the latter was obtained with a solid angle of 8.5 msr ($\theta = 5^\circ\text{--}6^\circ$). The energy accuracy and resolution, typically ~ 1 MeV, was limited primarily by that of the accelerator beam and somewhat by the solid-state telescope. A similar spectrum for $^{110}\text{Pd}(^{18}\text{O}, ^{20}\text{Ne})^{108}\text{Ru}$ is shown in Fig. 16.

The poor energy resolution is the result of tuning the accelerator for minimum time spread.³¹ At the beam line used, the phase-space limit for the beam is $\Delta E(\text{FWHM})\Delta t(\text{FWHM}) = 200 \text{ keV ns}$. Therefore, tuning the beam for optimal timing, viz. $\Delta t(\text{FWHM}) = 200\text{--}300$ ps, results in a significant degradation of the energy resolution. In many experiments this would not be a problem, but for experiments requiring both good E and good TOF resolutions, such as mass measurements, it is a problem. Such experiments should use a separate start detector and have the accelerator tuned for minimum ΔE . This would also minimize problems arising from a beam accelerated out of phase with the accelerator rf. The latter often causes background in the mass spectra from intense inelastic or single-nucleon transfer groups.

3. Kinematic shifts and corrections

As mentioned earlier, there is a correlation due to spherical aberration between the position of an ion at the detector and θ . In a nuclear reaction there is also a shift in ejectile energy with θ , called the kinematic shift ($dE/d\theta$). This implies that ions for a fixed Q -value reaction will have an energy spread due to the finite $\Delta\theta$ of the spectrometer entrance aperture. In addition, there should be a correlation between r and θ , and hence E and r , so that measurement of r can be used to determine θ and then correct for $dE/d\theta$. This is done routinely in magnetic dipole spectrometers. We have also verified this correction method¹⁸ for the solenoid spectrometer using $^{18}\text{O} + ^{26}\text{Mg}$ reaction products. However, although $dE/d\theta$ was clearly present for discrete groups and could be compensated, only a slight improvement in the energy resolution could be obtained because of the large intrinsic beam energy spread. Despite this, kinematic and other angle-dependent compensations appear to be quite feasible and would be important for larger solenoid magnets (see Sec. VI).

IV. OTHER APPLICATIONS

A. Radioactive beam production

A solenoid similar to the one used at ANL has been set up at the University of Notre Dame Tandem Van de Graaff

facility to produce and focus secondary radioactive beams at the focal plane. This spectrometer will be run in an asymmetric mode, with $z_{igt} = 50$ cm. This will increase the solid angle, with a corresponding decrease in the particle energies focusable (see Fig. 6). Instead of a detector, a secondary target is located at the focal plane inside of a large, secondary scattering chamber. This chamber contains an appropriate set of detectors to measure reactions induced by the secondary beam. As an example, a 100-pna ^7Li beam (35 MeV) incident on a 1-mg/cm² ^9Be production target should yield a secondary beam of about $10^5\text{--}10^6$ ^8Li ions per second ($T_{1/2} = 844$ ms), with a 500-keV energy spread, focused to a ~ 1 -cm-diam spot at the solenoid focal plane (Fig. 4). Secondary reactions such as ($^8\text{Li}, ^8\text{Li}^*$), ($^8\text{Li}, ^9\text{Li}$), ($^8\text{Li}, ^6\text{Li}$), etc. should then be feasible (see Table V) and would provide information on nuclear reactions and nuclear systems not presently accessible. Thus the study of nuclear reactions involving metastable nuclei important in astrophysics (nucleosynthesis) should be possible with such a system. Preliminary in-beam tests are in progress and will be reported elsewhere.

B. Production of polarized heavy ions

Nuclear reactions induced by a longitudinally polarized beam will normally result in an ejectile which may also be highly longitudinally polarized. Thus ($^3\text{He}, ^6\text{He}$) or ($^6\text{Li}, ^6\text{He}$) on appropriate targets would produce a secondary polarized ^6He beam at the solenoid focus with an intensity of $\sim 10^6$ particles/s. The axial field of the solenoid would not significantly depolarize a longitudinally polarized beam. This may prove to be another useful application of the large solid-angle solenoid lens.

V. MULTIPLE- q AND ACHROMATIC SYSTEMS

A. Long solenoid

An interesting property of Eq. (1) is that with a sufficiently long solenoid, viz. with focal length equal to that for charge state $q = 1$, all charge states of an ion at one energy can be brought simultaneously to a common focus.¹⁰ This can have applications in secondary-beam production (above), fragmentation studies,⁴ heavy-ion beam transport systems, and other situations in which a relatively monoenergetic, high- Z ion (such as a fusion product) has passed through a foil, resulting in a spread of ionic charge states.

B. Solenoid with radial E lens

Another potentially useful design combines a solenoid lens (axial B) with a radial electric-field lens (ELCO lens).¹¹ The latter can be used to partially compensate the chromatic or charge-state dispersion of the solenoid and thus produce a semiachromatic system.¹⁰ The ELCO lens can also be used to correct some of the spherical aberrations inherent in large-solid-angle designs (see Fig. 10). This again has applications for many types of heavy-ion experiments.

TABLE V. Radioactive beam experiments with estimated rates.

Radioactive beam	Production reaction	$E(\text{beam})^a$ (MeV)	Q (MeV)	Production rate (part/s) ^b	ΔE^c (MeV)	Secondary reaction	Q (MeV)	Event rate ^d (counts/sr h)
⁸ Li (844 ms)	² H(⁷ Li, ⁸ Li) ¹ H	25	- 0.2	2×10^6	1.0	¹² C(⁸ Li, ⁸ Li) ¹² C	0.0	4000
	⁹ Be(⁷ Li, ⁸ Li) ⁸ Be	25	+ 0.4	3×10^5	0.5	¹² C(⁸ Li, ⁸ Li*) ¹² C	< 0.0	400
	⁹ Be(⁶ Li, ⁸ Li) ⁷ Be	35	- 11.3	3×10^5	0.5	¹² C(⁸ Li, ⁶ Li) ¹⁴ C ¹² C(⁸ Li, ⁹ Li) ¹¹ C	3.8 - 14.7	4 20
⁷ Be (53.4 d)	¹ H(⁷ Li, ⁷ Be)n	25	- 1.6	2×10^6	1.0	¹² C(⁷ Be, ⁷ Be) ¹² C	0.0	4000
	⁹ Be(⁷ Li, ⁷ Be) ⁹ Li	35	- 14.5	3×10^5	0.5	¹² C(⁷ Be, ⁷ Be*) ¹² C	< 0.0	400
	⁹ Be(⁶ Li, ⁷ Be) ⁸ Li	35	- 11.3	3×10^5	0.5	¹² C(⁷ Be, ⁶ Li) ¹⁵ N ¹² C(⁷ Be, ⁸ B) ¹¹ B ⁷ Li(⁷ Be, ⁷ Be) ⁷ Li	- 3.7 - 15.8 0.0	20 8 4000
⁹ Li (177 ms)	⁹ Be(⁷ Li, ⁹ Li) ⁷ Be	35	- 14.5	3×10^5	0.5	¹² C(⁹ Li, ⁹ Li) ¹² C ⁹ Be(⁹ Li, ⁸ He) ¹⁰ B ¹¹ B(⁹ Li, ⁸ He) ¹² C	0.0 - 7.4 2.0	800 2 4
²⁰ O (13.5 s)	¹⁸ O(¹⁸ O, ²⁰ O) ¹⁶ O	25	- 0.6	1×10^5	0.4	¹² C(²⁰ O, ¹⁸ O) ¹⁴ C ¹² C(²⁰ O, ¹⁶ O) ¹⁶ C	1.6 - 5.2	0.5 0.1

^a Maximum consistent with solenoid focusing at $d = 2$ m.^b Rate for $d\Omega = 30$ msr, $\theta = 3^\circ$ - 6° , assuming $i = 100$ pna, $\rho x = 1$ mg/cm².^c Estimated energy spread at secondary target.^d Estimated secondary event rate ($d\Omega = 1$ sr) using a $\rho x = 1$ mg/cm² secondary target.

VI. VERY-LARGE-BORE AIR-CORE DESIGN

The present 0.2-m diam, 3.5-T magnet is limited to $E/A \leq 6$ MeV/u (see Table IV and Figs. 5 and 6). This E/A limit could be increased, e.g., doubled, by coupling two such magnets together.¹² However, one would like a system capable of focusing E/A up to 30 MeV/u, which is the energy needed to produce significant fragmentation yields of nuclei out to the neutron and proton drip lines.⁵

We have, therefore, studied the feasibility of using a large-bore, high-field, air-core solenoid for this purpose. Specifically, we have examined the characteristics of a 0.4-m bore, ~ 1 -m long, $B \geq 5$ T superconducting solenoid. Such a magnet is within the capabilities of several commercial manufacturers using standard Nb-Ti superconducting coil wire. [Magnets of this size with 7- to 9-T fields are also thought to be feasible, but would require special wire (Nb-Sn) and special quench protection, with a substantial increase in cost.] Preliminary design work indicates that such a magnet would be a very cost-effective system capable of focusing ions up to $E/A = 30$ MeV/u with a solid angle of $d\Omega \geq 20$ msr. Alternately, one could use the magnet with its large bore as a very-long-flight-path TOF spectrometer for high-mass ions, e.g., fusion products. Of course, spherical aberrations and the nonisochronism will impose a limit on the TOF resolution and, hence, mass resolution unless one measures θ also or utilizes compensating ELCO lenses or some other scheme.

The very large solid angle possible with a 0.4-m bore air-core magnet makes this magnet well suited as a secondary and radioactive beam collector. It could also be used as a heavy meson (kaon) collector for energies up to 200 MeV or so. Our group is completing a design study for such a system and will propose construction of this type of magnet as a heavy-ion fragment collector for E/A up to 30 MeV/u.

VII. CONCLUSIONS

We have demonstrated the feasibility of using a large, air-core, superconducting-solenoid magnet as a heavy-ion spectrometer near $\theta = 0^\circ$. There appear to be numerous other applications, such as secondary-beam production, for this type of magnet and for systems with or without radial electric lenses to produce charge focusing or semiachromatic focusing. Very-large-bore air-core spectrometers capable of bending ions $E/A \geq 30$ MeV/u with $d\Omega \geq 20$ msr appear to be feasible at moderate cost using commercially available air-core superconducting solenoid magnets.

ACKNOWLEDGMENTS

We thank B. Giagola, R. Pardo, C. Beck, M. Dowell, S. Shaheen, L. Welch, and T. Moog for their assistance and comments. This work was supported in part by the U. S. National Science Foundation Grants Nos. PHY-83-08072, PHY-84-16025, and PHY-86-05907, the U.S. Department of Energy Grant No. W-31-109-ENG-38, and the Thesis Grant program of ANL's Department of Educational Programs.

^{a)} Permanent address: Eastman Kodak Co., 343 State St., Rochester, New York 14650.

^{b)} Permanent address: Machine Vision International, 325 E. Eisenhower Parkway, Ann Arbor, Michigan 48104.

^{c)} Permanent address: Department of Physics, University of Richmond, Richmond, Virginia 23173.

^{d)} On leave from Physics Department, University of Manchester, Manchester, England.

¹H. J. Rose and G. A. Jones, *Nature* **307**, 245 (1984).

²*Heavy-Ion Collisions*, edited by R. Bock (North-Holland, Amsterdam, 1980), Vols. 1-3.

³I. Paschopoulos, E. Müller, H. J. Körner, I. C. Oelrich, K. E. Rehm, and H. J. Scheerer, *Phys. Rev. C* **18**, 1277 (1978); H.-P. Rother, W. Henning, H.-J. Körner, R. Müller, K. E. Rehm, M. Richter, and H. Spieler, *Nucl. Phys. A* **269**, 511 (1976); T. S. Bhatia, H. Hafner, R. Haupt, R. Maschuw, and G. J. Wagner, *Z. Phys. A* **281**, 65 (1977); R. Haupt, C.-A. Wiedner, G. J. Wagner, K. Wannebo, T. S. Bhatia, H. Hafner, R. Maschuw, W. Saathoff, and S. T. Thornton, *Z. Phys. A* **317**, 193 (1984); J. P. Dufour, R. Del Moral, H. Emmermann, F. Hubert, D. Jean, C. Poinot, M. S. Pravikoff, A. Fleury, H. Delagrange, and K.-H. Schmidt, *Nucl. Instrum. Methods A* **248**, 267 (1986).

⁴J. C. Peng, N. Stein, J. W. Sunier, D. M. Drake, J. D. Moses, J. A. Cizewski, and J. R. Tesmer, *Phys. Rev. Lett.* **43**, 675 (1979); M. Bernas, P. Dessagne, M. Langevin, J. Payet, F. Pougheon, P. Roussel, W.-D. Schmidt-OH, P. Tidemand-Petersson, and M. Girod, *Nucl. Phys. A* **413**, 363 (1984); M. C. Cohler, D. L. Watson, R. Wadsworth, S. M. Lane, M. J. Smithson, R. E. Brown, J.-C. Peng, N. Stein, J. W. Sunier, and D. M. Drake, *Z. Phys. A* **319**, 107 (1984); W. A. Mayer, W. Henning, R. Holzworth, H. J. Körner, G. Korschinek, W. U. Mayer, G. Rosner, and H. J. Scheerer, *Z. Phys. A* **319**, 287 (1984).

⁵A. G. Artukh, V. V. Audeichikov, G. F. Gridnev, V. L. Nikheev, V. V. Volkov, and J. Wilczynski, *Nucl. Phys. A* **176**, 284 (1971); M. Langevin, E. Quiniou, M. Bernas, J. Galin, J. C. Jacmart, F. Navlin, F. Pougheon, R. Anne, C. Détraz, D. Guerreau, D. Guillemaud-Mueller, and A. C. Mueller, *Phys. Lett.* **150B**, 71 (1985); D. Guillemaud-Mueller, A. C. Mueller, D. Guerreau, F. Pougheon, R. Anne, M. Bernas, J. Galin, J. C. Jacmart, M. Langevin, F. Navlin, E. Quiniou, and C. Détraz, *Z. Phys. A* **322**, 415 (1985).

⁶J. P. Schapira, F. Azaiez, S. Fortier, S. Gales, E. Hourani, J. Kumpulainen, and J.-M. Maison, *Nucl. Instrum. Methods* **224**, 337 (1984).

⁷R. Stern, F. Becchetti, T. Casey, J. Jänecke, P. Lister, D. Kovar, R. Janssens, R. Pardo, M. Vineyard, and J. Kolata, *Proceedings of the Conference on Instrumentation for Heavy-Ion Nuclear Research*, edited by D. Schapira, ORNL Publ. Conf.-841005, abstract, 1984, p. 95.

⁸S. Gales, E. Hourani, M. Hussonnois, J.-P. Schapira, L. Stab, and M. Vergnes, *Phys. Rev. Lett.* **53**, 759 (1984).

⁹F. D. Becchetti and J. Jänecke, Proposal UMNP-BE-85-15, Univ. of Michigan, 1985, *Proceedings of the Accelerated Radioactive Beams Workshop*, edited by L. Buchman and J. M. Auria (TRIUMF, Vancouver, BC, 1985); *Proceedings of the Workshop on Radioactive Beams and Small Cross Sections*, edited by R. N. Boyd (Ohio State Univ., Columbus, OH, 1981); *Proceedings of the Workshop on Prospects for Research with Radioactive Beams from Heavy Ion Accelerators*, edited by J. M. Nitschke (LBL-18187:59, Washington, DC, 1984).

¹⁰W. Z. Liu, R. Stern and F. D. Becchetti, *Rev. Sci. Instrum.* **58**, 220 (1987).

¹¹P. Krejcik, R. L. Dalglis, and J. C. Kelly, *J. Phys. D* **12**, 161 (1979); P. Krejcik, J. C. Kelly, and R. L. Dalglis, *Nucl. Inst. Methods* **168**, 247 (1980); P. Krejcik, B. V. King, and J. C. Kelly, *Optik* **55**, 385 (1980).

¹²J. P. Schapira, S. Gales, and H. Laurent, Orsay Report IPNO-PhN-7921, 1979; English translation by E. Charnock and R. Stern, Univ. of Michigan, UM-BE-10, 1985 (unpublished).

¹³V. E. Cosslett, *Introduction to Electron Optics* (Clarendon, Oxford, 1950); P. Grivet, *Electron Optics* (Pergamon, New York, 1965); W. Glaser, *Grundlagen der Elektronenoptik* (Springer, Vienna, 1952).

¹⁴K. Siegbahn, *Alpha, Beta, and Gamma Ray Spectroscopy* (North-Holland, Amsterdam, 1965).

¹⁵D. J. Decman, E. A. Henry, J. Kantele, L. G. Mann, W. Stöfl, R. J. Estep, and L. E. Ussery, *Nucl. Instrum. Methods* **219**, 523 (1984); W. Stöfl and E. A. Henry, *Nucl. Instrum. Methods* **227**, 77 (1984); M. Guttormsen, H. Hübel, A. V. Grumbkow, Y. K. Agarwal, J. Recht, K. H. Maier, H. Kluge, A. Maj, M. Menningen, and N. Roy, *Nucl. Instrum. Methods* **227**, 489 (1984).

¹⁶D. Johnson, E. Kashy, and J. A. Nolen, MSU-NSCL Rep. 222, 1976 (unpublished).

¹⁷H. Laruent and J. P. Schapira, *Nucl. Instrum. Methods* **162**, 181 (1979).

- ¹⁸Robin Stern, Ph.D. thesis, Univ. of Michigan, 1987 (unpublished).
- ¹⁹Intermagetics General Corporation, Guilderland, NY.
- ²⁰F. D. Becchetti and E. Sweetman, *Bull. Am. Phys. Soc.* **28**, 698 (1983).
- ²¹Ohio Semitronics, Inc., Columbus, OH.
- ²²CAJON Co., Macedonia, OH.
- ²³Z. Liu, W. Henning, B. Glagola, J. G. Keller, W. Kutschera, K. E. Rehm, and R. H. Siemssen, *Bull. Am. Phys. Soc.* **31**, 820 (1986); W. Henning, M. Paul, W. Kutschera, K. E. Rehm, and R. H. Siemssen, *Bull. Am. Phys. Soc.* **30**, 1249 (1985).
- ²⁴R. Stern, F. Becchetti, J. Jänecke, P. Lister, W. Phillips, D. Kovar, M. Vineyard, and J. Kolata, *Bull. Am. Phys. Soc.* **31**, 819 (1986).
- ²⁵Buckbee-Mears Inc., St. Paul, MN.
- ²⁶ORTEC Inc., Oak Ridge, TN.
- ²⁷J. Walton, Detector Group, Lawrence Berkeley Laboratory, Berkeley, CA.
- ²⁸J. Aron, R. Benaroya, J. Bogaty, L. M. Bollinger, B. E. Clift, P. Den Hartog, K. W. Johnson, W. Kutschera, P. Markovich, J. M. Nixon, R. C. Pardo, K. W. Shepard, and G. Zinkman, *Rev. Sci. Instrum.* **57**, 737 (1986).
- ²⁹Robert L. Fleischer, P. Buford Price, and Robert M. Walker, *Nuclear Tracks in Solids* (Univ. of California, Berkeley, CA, 1975).
- ³⁰CRONAR unsensitized C42 0.1-mm graphics art film, Dupont, Inc., Wilmington, DE.
- ³¹L. M. Bollinger (personal communication, 1986).